Inorganic Chemistry

Article

pubs.acs.org/IC

Influence of Photoinduced Electron Transfer on Lanthanide-Based Coordination Polymer Luminescence: A Comparison between Two Pseudoisoreticular Molecular Networks

Stéphane Freslon,[†,‡] Yun Luo,[†,‡] Guillaume Calvez,[†,‡] Carole Daiguebonne,*[,†,‡] Olivier Guillou,*[,†,‡] Kevin Bernot,[†,‡] Vincent Michel,[†,‡] and Xiao Fan[†,‡]

[†]Université Européenne de Bretagne, 5 Boulevard Laënnec, 35000 Rennes, France

[‡]INSA, UMR 6226 "Institut des Sciences Chimiques de Rennes", 20, Avenue des Buttes de Coesmes, F-35708 Rennes, France

Supporting Information

ABSTRACT: The luminescent properties of two families of heteronuclear lanthanide-containing coordination polymers are compared. These families have general chemical formulas $[Ln_{2-2x}Ln'_{2x}(ip)_3(H_2O)_9{\cdot}6H_2O]_\infty$ and $[Ln_{2-2x}Ln'_{2x}(aip)_2(H_2O)_{10}{\cdot}(aip){\cdot}4H_2O]_\infty$ where H_2ip and H_2aip stand for isophthalic acid and 5-amino-isophthalic acid, respectively, and where Ln and Ln′ are one of the lanthanide ions between Sm^{3+} and Dy^{3+}. Heteronuclear compounds that belong to each family are isostructural to the already reported homonuclear compounds $[Gd_2(ip)_3(H_2O)_9{\cdot}6H_2O]_\infty$ and $[Eu_2(aip)_2(H_2O)_{10}{\cdot}(aip){\cdot}4H_2O]_\infty$, respectively. These two crystal structures are very similar. However, despite similar chemical formulas, similar crystal structures, and similar hydration rates, these two families of compounds present very different luminescent properties that have thus been deeply investigated. This study demonstrates that these different optical behaviors can be attributed to the presence of a PET (photoinduced electron transfer) mechanism that is only present in the amino-isophthalate-containing coordination polymers.

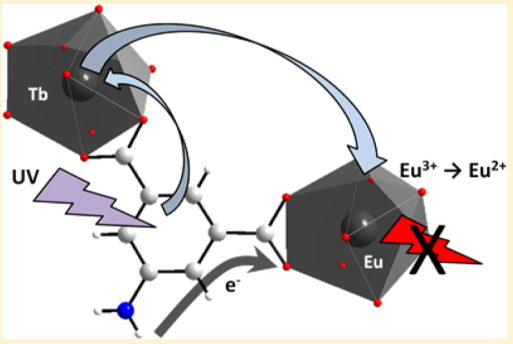

INTRODUCTION

For more than a decade, lanthanide-containing coordination polymers have attracted great attention because of their potential applications[1,2] in gas storage,[3−11] catalysis,[12] separation,[13] molecular magnetism,[14−16] or luminescence.[17−23] Actually, due to the inner character of their valence orbitals, lanthanide ions have similar chemical properties, and it is possible to synthesize coordination polymers in which two or more lanthanide ions are randomly distributed over the metallic sites.[24,25] This enables one to tune the intermetallic distances and therefore to modulate the color and the brightness of emission.[26−30] In the past few years it has been demonstrated that heteronuclear lanthanide-based coordination polymers present high potential as far as luminescent properties are targeted.[24,31−35] Despite this obvious advantage, there are only few heteronuclear compounds described to date.[24−32,36,37]

For almost a decade our group is involved in the synthesis of benzene-polycarboxylate lanthanide-based coordination polymers.[38,39] In the frame of this work, we have obtained two families of isostructural compounds[40,41] with respective general chemical formulas $[Ln_2(ip)_3(H_2O)_9{\cdot}6H_2O]_\infty$ and $[Ln_2(aip)_2(H_2O)_{10}{\cdot}aip){\cdot}4H_2O]_\infty$ where H_2ip and H_2aip stand for isophthalic acid and 5-amino-isophthalic acid, respectively (Scheme 1), and where Ln and Ln′ are lanthanide ions falling between Sm^{3+} and Dy^{3+}.

Surprisingly, these two families of compounds present very similar crystal structures that can be described as a juxtaposition of stairlike molecular double chains motifs, but very different luminescence properties (see Supporting Information Figures S1 and S2).

Scheme 1. (Left) Isophtalic Acid (1,3-Benzene-di-carboxylic Acid) Abbreviated $H_2(ip)$ and (Right) Amino-isophtalic Acid (5-Amino-1,3-benzene-di-carboxylic Acid) Abbreviated $H_2(aip)$

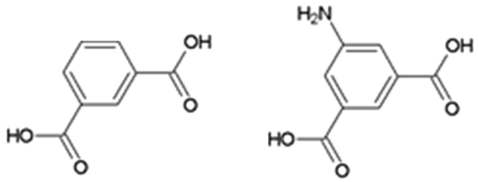

In both crystal structures there are two crystallographically independent lanthanide ions that are nine-coordinated.

In $[Gd_2(ip)_3(H_2O)_9{\cdot}6H_2O]_\infty$, Gd1 is linked to four oxygen atoms from two bidentate carboxylate groups and five oxygen atoms from five coordination water molecules. Gd2 is also coordinated to four oxygen atoms that belong to bidentate carboxylate groups and four oxygen atoms from coordination water molecules. The ninth oxygen atom belongs to a monodentate

Received: November 13, 2013
Published: January 8, 2014

   dx.doi.org/10.1021/ic402841d | *Inorg. Chem.* 2014, 53, 1217−1228

Table 1. Elemental Analyses for $[Ln_2(ip)_3(H_2O)_9{\cdot}6H_2O]_\infty$ with Ln = Sm−Dy

		calcd (found) %			
	MW (g mol^{-1})	Ln	C	O	H
$[Sm_2(ip)_3(H_2O)_9{\cdot}6H_2O]_\infty$	1063.29	28.3 (28.2)	27.1 (27.2)	40.6 (40.4)	4.0 (4.2)
$[Eu_2(ip)_3(H_2O)_9{\cdot}6H_2O]_\infty$	1066.50	28.5 (28.5)	27.0 (27.1)	40.5 (40.5)	4.0 (3.9)
$[Gd_2(ip)_3(H_2O)_9{\cdot}6H_2O]_\infty$	1077.07	29.2 (29.4)	26.8 (26.8)	40.1 (40.0)	3.9 (3.8)
$[Tb_2(ip)_3(H_2O)_9{\cdot}6H_2O]_\infty$	1080.42	29.4 (29.4)	26.7 (26.7)	40.0 (39.8)	3.9 (4.1)
$[Dy_2(ip)_3(H_2O)_9{\cdot}6H_2O]_\infty$	1087.57	29.9 (29.8)	26.5 (26.4)	39.7 (39.7)	3.9 (3.7)

Table 2. Elemental Analyses for $[Ln_2(aip)_3(H_2O)_{10}{\cdot}(aip){\cdot}4H_2O]_\infty$ with Ln = Sm−Dy

		calcd (found) %				
	MW (g mol^{-1})	Ln	C	N	O	H
$[Sm_2(aip)_3(H_2O)_{10}{\cdot}(aip){\cdot}4H_2O]_\infty$	1269.45	23.7 (23.7)	30.3 (30.4)	4.4 (4.3)	37.8 (37.9)	3.8 (3.7)
$Eu_2(aip)_3(H_2O)_{10}{\cdot}(aip){\cdot}4H_2O]_\infty$	1272.66	23.9 (23.8)	30.2 (30.1)	4.4 (4.5)	37.7 (37.8)	3.8 (3.8)
$[Gd_2(aip)_3(H_2O)_{10}{\cdot}(aip){\cdot}4H_2O]_\infty$	1283.23	24.5 (24.6)	29.9 (30.0)	4.4 (4.4)	37.4 (37.3)	3.8 (3.7)
$[Tb_2(aip)_3(H_2O)_{10}{\cdot}(aip){\cdot}4H_2O]_\infty$	1286.58	24.7 (24.7)	29.9 (30.0)	4.3 (4.2)	37.3 (37.4)	3.8 (3.7)
$[Dy_2(aip)_3(H_2O)_{10}{\cdot}(aip){\cdot}4H_2O]_\infty$	1293.73	25.2 (25.2)	29.7 (29.9)	4.3 (4.3)	37.1 (37.0)	3.7 (3.6)

carboxylate group of an isophthalate ligand that lies in the interchain space. The second carboxylate group of this ligand is not bounding. The two coordination polyhedrons are best described by tricapped trigonal prism. Globally, in this crystal structure, the two Gd^{3+} ions are linked to nine coordination water molecules, and six crystallization water molecules are located between the chains.

In $[Eu_2(aip)_2(H_2O)_{10}{\cdot}(aip){\cdot}4H_2O]_\infty$, both Eu^{3+} ions are linked to four oxygen atoms from two bidentate carboxylate groups and five oxygen atoms from coordination water molecules. The two coordination polyhedrons are best described by tricapped trigonal prism. Overall, in this crystal structure, the two Eu^{3+} ions are linked to 10 coordination water molecules, and 4 crystallization water molecules are located between the chains. Therefore, hydration rates are close in both crystal structures. Actually, the main difference with the previous crystal structure is that, in this crystal structure, the amino-isophthalate ligand that lies in the interchain space is not bounded to the molecular skeleton.

It can be noticed that, upon UV irradiation of the ligand, both Tb-containing compounds exhibit strong green luminescence (Supporting Information Figures S1 and S2). On the other hand, only the isophthalate-based Eu-containing compound, $[Eu_2(ip)_3(H_2O)_9{\cdot}6H_2O]_\infty$, exhibits red luminescence while the amino-isophthalate-based one, $[Eu_2(aip)_2(H_2O)_{10}{\cdot}(aip){\cdot}4H_2O]_\infty$, exhibits almost no luminescence. In order to understand why these two almost isoreticular families of compounds exhibit such different luminescent properties we have undertaken the synthesis of heteronuclear members of both series. Indeed, it has been proven that the study of heterolanthanide-based coordination polymers is useful for understanding the different mechanisms involved in their luminescence.[26,29]

EXPERIMENTAL SECTION

Synthesis of the Microcrystalline Powders. 1,3-Benzenedicarboxylic and 5-amino-1,3-benzene-dicarboxylic acids were purchased from Acros Organics and used without further purification. Their disodium salts were prepared by addition of 2 equiv of sodium hydroxide to aqueous suspensions of acids. Then, the obtained clear solutions were evaporated to dryness. The resulting solids were suspended in small amounts of ethanol. The mixtures were stirred and refluxed for 1 h. Upon addition of ethoxyethane, precipitations occurred. After filtration and drying, white powders of the disodium salts were obtained in 90% yields. For $Na_2(ip){\cdot}H_2O$, $C_8H_6O_5Na_2$ (MW = 228 g mol^{-1}) Anal. Calcd (Found): C 45.7% (45.5%); H 1.9% (2.0%); O 30.5% (30.6%); Na 21.9% (21.9%).

For $Na_2(aip){\cdot}H_2O$, $C_8H_7NO_5Na_2$ (MW = 243 g mol^{-1}) Calcd (Found): C 42.5% (42.5%); H 2.7% (2.6%); N 6.2% (6.3%); O 28.3% (28.2%); Na 20.3% (20.4%).

Hydration rates of the two salts have been confirmed by TGA (Supporting Information Figures S3 and S4).

Hydrated lanthanide chlorides were prepared from the corresponding oxides according to literatures methods.[39] Lanthanide oxides were purchased from STREM Chemicals and used without further purification.

Microcrystalline powders of the homonuclear coordination polymers were obtained as already described.[40,41] The obtained microcrystalline powders have been assumed to be isostructural to the single crystals on the basis of their X-ray powder diffraction diagrams (Supporting Information Figure S5). Results of the elemental chemical analyzes are listed in Tables 1 and 2.

Microcrystalline powders of the heteronuclear compounds have been obtained according to similar procedures by simply replacing the lanthanide chloride solution by the appropriate mixture of lanthanide chloride solutions in the synthetic processes. The obtained microcrystalline powders have been assumed to be isostructural to the corresponding homonuclear compounds, on the basis of their X-ray powder diffraction diagrams. For example, X-ray diffraction patterns for some heteronuclear compounds are reported in Supporting Information Figure S6.

For heteronuclear compounds the relative ratios between the two different lanthanide ions have been measured by EDS. Some results are listed in Table 3.

X-ray Powder Diffraction. The diagrams have been collected using a Panalytical X'Pert Pro diffractometer with an X'Celerator detector. The typical recording conditions were 40 kV, 40 mA for Cu Kα (λ = 1.542 Å), and the diagrams were recorded in θ/θ mode for 60 min between 5° and 75° (8378 measurements) with a step size of 0.0084° and a scan time of 50 s. The calculated patterns were produced using the Powdercell and WinPLOTR software programs.[42−44]

FT-IR Measurements. FT-IR measurements have been performed on KBr pellets between 400 and 4000 cm^{-1} using a Perkin-Elmer Paragon 1000 PC spectrometer. For both series of compounds, the IR spectra support the crystal structure. Actually all spectra clearly show the characteristic band for deprotonated carboxylato groups (1380 cm^{-1}) and not for protonated carboxylato groups (1410 cm^{-1}). The characteristic band for $-NH_2$ at 1610 cm^{-1} is also observed for compounds that constitute the amino-isophthalate-based family.

Energy Dispersive Spectroscopy. All EDS measurements were carried out with a Hitachi TM-1000, Tabletop Microscope version 02.11 (Hitachi High-Technologies, Corporation, Tokyo, Japan) with EDS analysis system (SwiftED-TM, Oxford Instruments Link INCA). The

dx.doi.org/10.1021/ic402841d | Inorg. Chem. 2014, 53, 1217−1228

Table 3. Relative Ratios between Ln and Ln′ for Some $[Eu_{2-2x}Tb_{2x}(ip)_3(H_2O)_9{\cdot}6H_2O]_\infty$ and $[Eu_{2-2x}Tb_{2x}(aip)_2(H_2O)_{10}{\cdot}(aip){\cdot}4H_2O]_\infty$

$[Eu_{2-2x}Tb_{2x}(ip)_3(H_2O)_9{\cdot}6H_2O]_\infty$			$[Eu_{2-2x}Tb_{2x}(aip)_2(H_2O)_{10}{\cdot}(aip){\cdot}4H_2O]_\infty$		
Tb (%)[a]	Eu (%)[a]	x[b]	Tb (%)[a]	Eu (%)[a]	x[b]
100(2)	0(2)	1.00	100(2)	0(2)	1.00
91(2)	9(2)	0.90	89(2)	11(2)	0.90
81(2)	19(2)	0.80	78(2)	22(2)	0.80
71(2)	29(2)	0.70	72(2)	28(2)	0.70
59(2)	41(2)	0.60	57(2)	43(2)	0.60
48(2)	52(2)	0.50	45(2)	55(2)	0.50
41(2)	59(2)	0.40	40(2)	60(2)	0.40
33(2)	67(2)	0.30	27(2)	73(2)	0.30
23(2)	77(2)	0.20	25(2)	75(2)	0.20
10(2)	90(2)	0.10	10(2)	90(2)	0.10
0(2)	100(2)	0.00	0(2)	100(2)	0.00

[a]Experimental values (metal fractions found by elemental analyses). [b]Theoretical values (metal fractions used during the syntheses).

detector is a silicon drift detector, with an energy resolution of 165 eV which allows us to detect the element from Na to U. With the software SwiftED-TM, qualitative and quantitative analyses can be performed. All the samples have been observed by means of an electron beam accelerated at 15 kV, under high vacuum. The samples were assembled on carbon discs, stuck on an aluminum stub fixed at 7 mm from EDX beam, with an angle of measurement of 22°. Reproducibility of the elemental analyses was carefully checked by reproducing several times the measurements on different takings for each sample. These measurements, as well as the pictures (see for example Supporting Information Figure S7), strongly support the monophasic character of all samples.

Solid State Luminescent Measurements. Solid state emission spectra were measured on a Horiba Jobin-Yvon Fluorolog III fluorescence spectrometer with a pulsed Xe lamp. Slit widths for excitation and emission were 2 nm for the Eu- and Tb-containing compounds and 5 nm for the Sm- and Dy-containing compounds. Almost all luminescence spectra were recorded at room temperature between 450 and 800 nm except for $[Eu_2(aip)_3(H_2O)_{10}{\cdot}(aip){\cdot}4H_2O]_\infty$ for which it has also been recorded at 77 K. The data were collected at every nanometer with an integration time of 100 ms for each step. The quantum yield measurements were performed using a Jobin−Yvon integrating sphere [$\Phi = (E_c - E_a)/(L_a - L_c)$ with E_c being the integrated emission spectrum of the sample, E_a the integrated "blank" emission spectrum, L_a the "blank" absorption, and L_c the sample absorption at the excitation wavelength].

Comparative solid state luminescent spectra were measured on a Perkin-Elmer LS-55 spectrometer between 450 and 800 nm under identical operating conditions and without turning the lamp off to ensure a valid comparison between the emission spectra. Reproducibility of the measurements as well as surface states of the samples (1.5 cm^2 pellets) have been carefully checked. Slit widths for excitation and emission were 5 or 10 nm depending on the series of samples.

The solid state luminescence spectra of the homonuclear Gd-containing compounds were recorded at 77 K in order to obtain the energy levels of the lowest triplet states of the ligands (see Supporting Information Figures S8 and S9).

Luminescence intensities of the samples expressed in Cd m^{-2} have been measured with a Gigahertz-Optik X1-1 optometer with an integration time of 200 ms on 1.5 cm^2 pellets. The intensity of the UV flux, 2.5(1) W m^{-2}, was measured with a Vilber Lourmat VLX-3W radiometer.

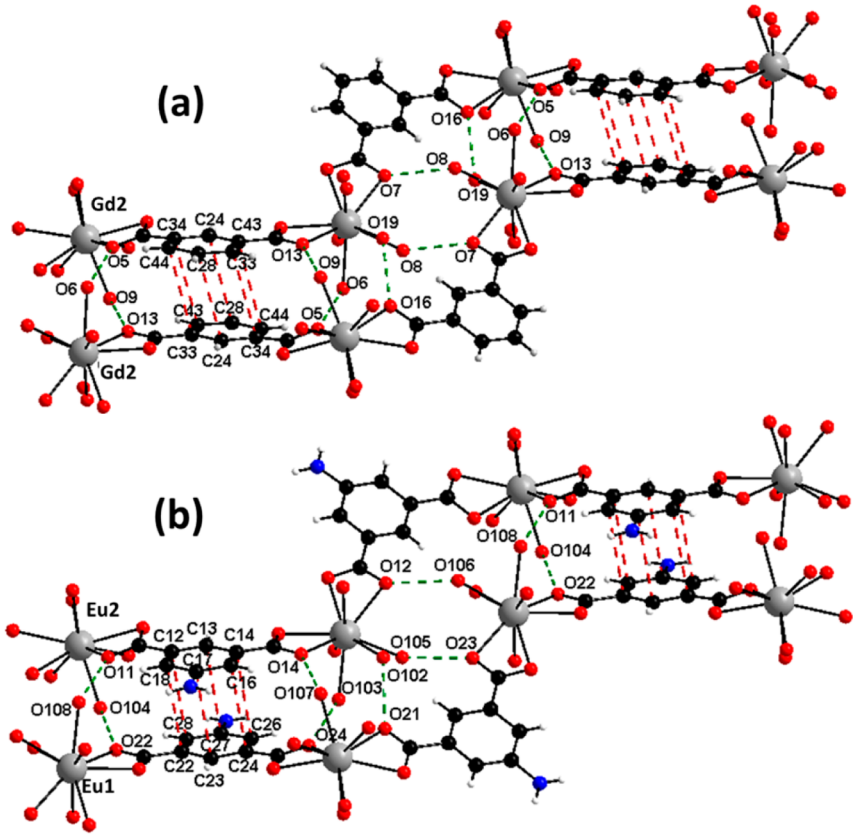

Figure 1. Projection views of the stair-like double molecular chains of $[Gd_2(ip)_3(H_2O)_9{\cdot}6H_2O]_\infty$ (a) and of $[Eu_2(aip)_2(H_2O)_{10}{\cdot}(aip){\cdot}4H_2O]_\infty$ (b). Hydrogen bonds and π-stacking interactions are symbolized by dotted lines.

dx.doi.org/10.1021/ic402841d | Inorg. Chem. 2014, 53, 1217−1228

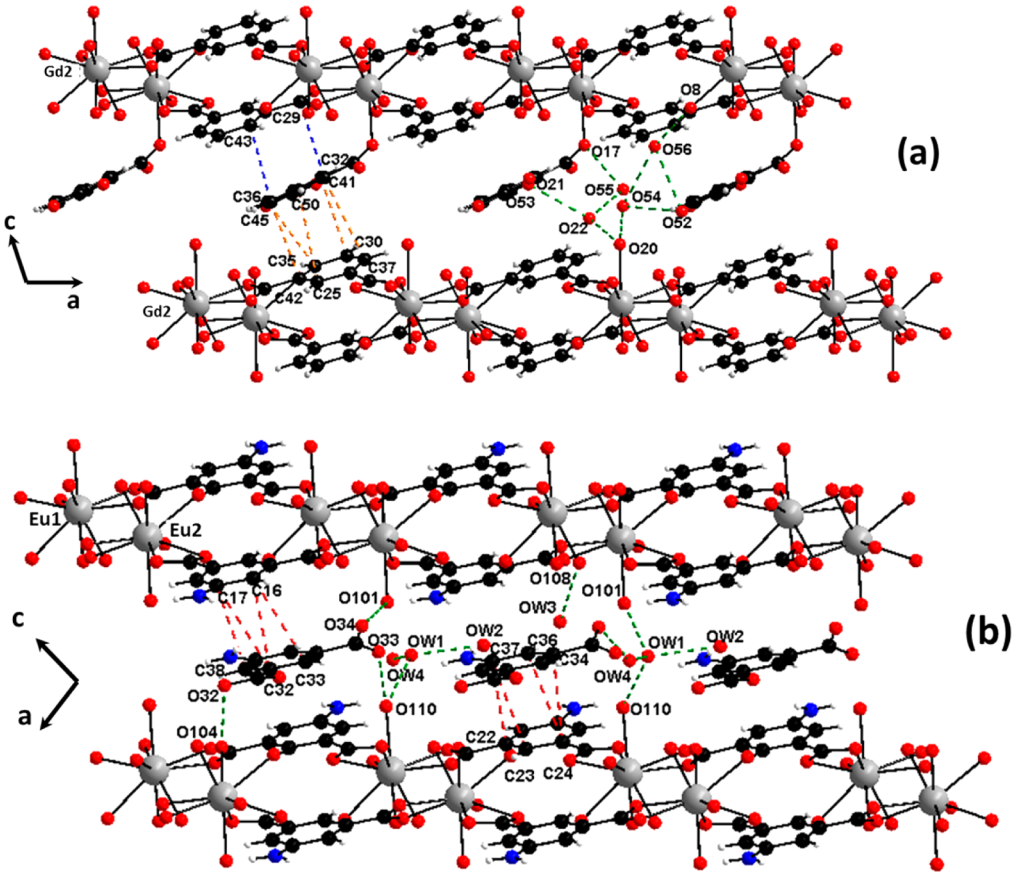

Figure 2. Projection views along the *b* axis of the packing of two double-chain motifs of $[Gd_2(ip)_3(H_2O)_9{\cdot}6H_2O]_\infty$ (a) and of $[Eu_2(aip)_2(H_2O)_{10}{\cdot}(aip){\cdot}4H_2O]_\infty$ (b). Hydrogen bonds and π-stacking interactions are symbolized by dotted lines.

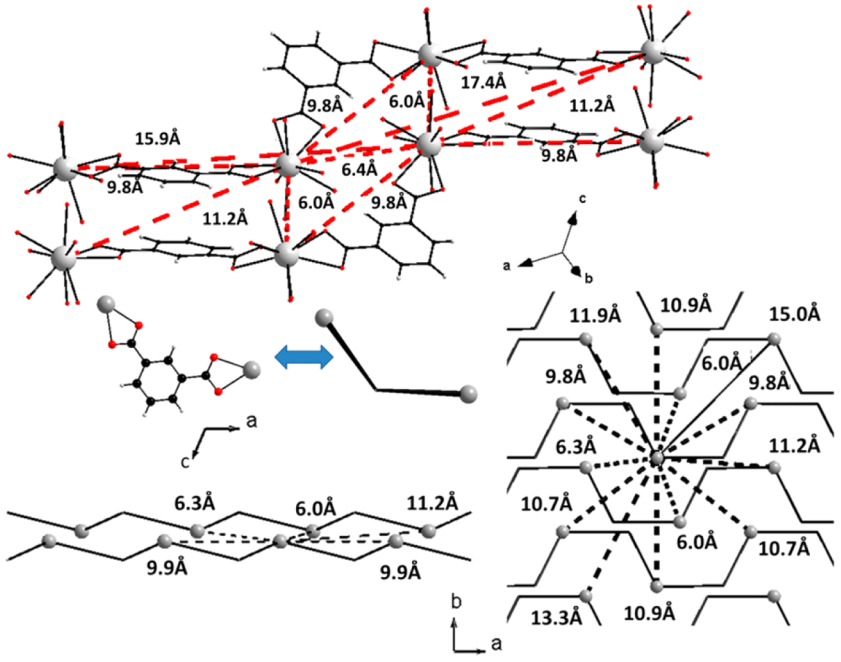

Figure 3. Intermetallic distances between Gd atoms that belong to the same molecular motif in $[Gd_2(ip)_3(H_2O)_9{\cdot}6H_2O]_\infty$. Distances are listed in Supporting Information Table S7.

UV−Vis Absorption Measurements. UV−vis absorption spectra were recorded on a Perkin-Elmer Lambda 650 spectrometer. Solid state measurements were recorded using a praying mantis unit. Solid state UV−vis absorption spectra of the Gd-containing compounds have been recorded for estimating the energy of the lowest singlet excited states of the ligands. Liquid state measurements were performed for evaluating

dx.doi.org/10.1021/ic402841d | *Inorg. Chem.* 2014, 53, 1217−1228

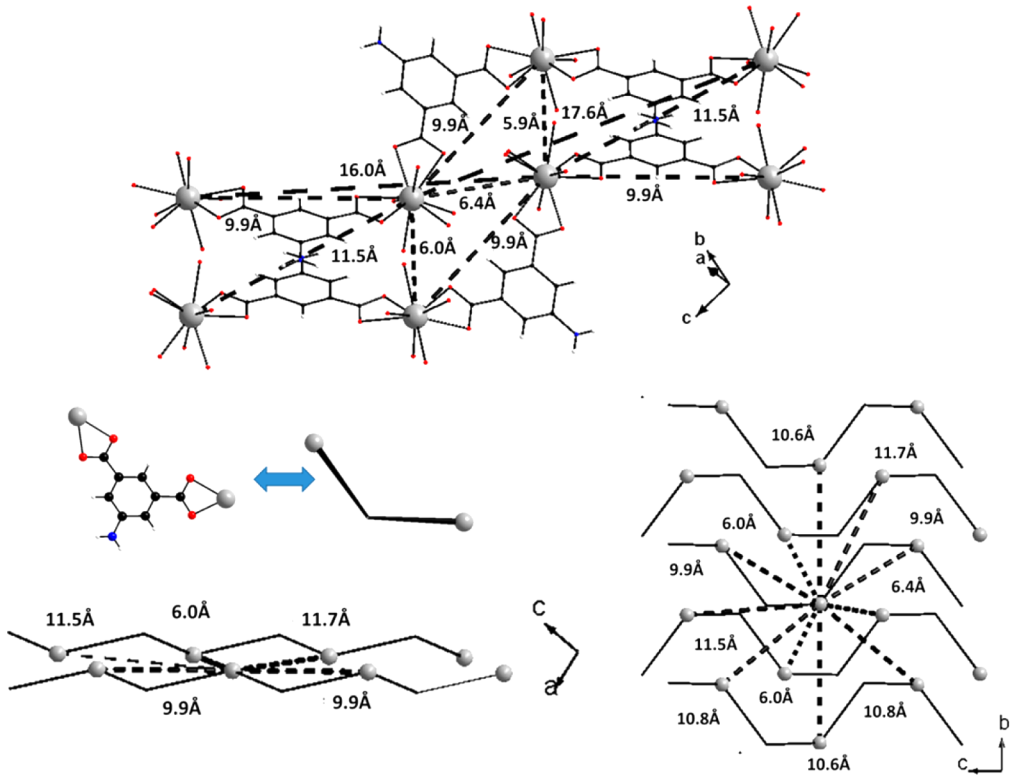

Figure 4. Intermetallic distances between Eu atoms that belong to the same molecular motif in $[Eu_2(aip)_2(H_2O)_{10}\cdot(aip)\cdot 4H_2O]_\infty$. Distances are listed in Supporting Information Table S8.

Table 4. Shortest Intermetallic Distances (<11 Å) between Lanthanide Ions That Belong to Different Double-Chain Molecular Motifs for $[Gd_2(ip)_3(H_2O)_9\cdot 6H_2O]_\infty$ (Top) and $[Eu_2(aip)_2(H_2O)_{10}\cdot(aip)\cdot 4H_2O]_\infty$ (Bottom)

atom1	atom2	symmetry	distance (Å)
Gd1	Gd2	$-1.5 + x, -0.5 - y, -1 + z$	10.274(1)
Gd1	Gd2	$-1.5 + x, -0.5 - y, -1 + z$	10.446(1)
Gd1	Gd2	$1.5 - x, 1.5 + y, 2 - z$	10.464(1)
Gd1	Gd2	$-1.5 + x, -0.5 - y, -1 + z$	10.515(1)
Gd1	Gd1	$-1 + x, 2 + y, -1 + z$	10.541(1)
Eu1	Eu2	x, y, z	8.721(1)

Table 5. Spectroscopic Data for $[Ln_2(ip)_3(H_2O)_9\cdot 6H_2O]_\infty$ with Ln = Sm, Eu, Tb, and Dy

	Q_{Ln}^{ligand}(%)	τ_{obs} (ms)
$[Sm_2(ip)_3(H_2O)_9\cdot 6H_2O]_\infty$	0.3(1)	0.007(1)
$[Eu_2(ip)_3(H_2O)_9\cdot 6H_2O]_\infty$	10(1)	0.19(2)
$[Tb_2(ip)_3(H_2O)_9\cdot 6H_2O]_\infty$	28(2)	0.60(6)
$[Dy_2(ip)_3(H_2O)_9\cdot 6H_2O]_\infty$	0.8(1)	0.23(2)

molar absorption coefficients of the ligands (see Supporting Information Figures S10 and S11).

Colorimetric Measurements. The CIE (Commission Internationale de l'Eclairage) (x, y) emission color coordinates[45,46] were obtained using a MSU-003 colorimeter (Majantys) with the PhotonProbe 1.6.0 software (Majantys). Color measurements: 2°, CIE 1931, step 5 nm, under 312 nm UV light. $X = k \times \int_{380nm}^{780nm} I_\lambda \times x_\lambda$, $Y = k \times \int_{380nm}^{780nm} I_\lambda \times y_\lambda$, and $Z = k \times \int_{380nm}^{780nm} I_\lambda \times z_\lambda$ with k constant for the measurement system I_λ sample spectrum intensity, wavelength depending, $x_\lambda, y_\lambda, z_\lambda$ trichromatic values $x = X/(X + Y + Z)$, $y = Y/(X + Y + Z)$, and $z = Z/(X + Y + Z)$. Mean xyz values are given for each sample, which act as light sources (luminescent samples). Standards from Phosphor Technology used as follows, calibrated at 312 nm: red phosphor Gd_2O_2S:Eu ($x = 0.667$, $y = 0.330$) and green phosphor Gd_2O_2S:Tb ($x = 0.328$, $y = 0.537$).

Table 6. Spectroscopic Data for $[Eu_2(ip)_3(H_2O)_9\cdot 6H_2O]_\infty$ and $[Tb_2(ip)_3(H_2O)_9\cdot 6H_2O]_\infty$

	Q_{Ln}^{ligand} (%)	τ_{obs} (ms)	Q_{Ln}^{Ln} (%)[b]	η_{sens} (%)[a]	τ_{rad} (ms)[a]
$[Eu_2(ip)_3(H_2O)_9\cdot 6H_2O]_\infty$	10(1)	0.19(2)	11(1)	90	1.7
$[Tb_2(ip)_3(H_2O)_9\cdot 6H_2O]_\infty$	28(2)	0.60(6)	32(3)	87	1.9

[a]Errors on calculated η_{sens} and τ_{rad} can be estimated to 15%. [b]Q_{Eu}^{Eu} and Q_{Tb}^{Tb} have been estimated on the basis of emission spectra recorded at 395 nm ($^5D_3$ energy level for Eu^{3+}) and 380 nm ($^5D_3$ energy level for Tb^{3+}), respectively.

Table 7. Spectroscopic Data for $[Ln_2(aip)_3(H_2O)_{10}\cdot(aip)\cdot 4H_2O]_\infty$ with Ln = Sm, Tb, and Dy

	Q_{Ln}^{ligand} (%)	τ_{obs} (ms)
$[Sm_2(aip)_3(H_2O)_{10}\cdot(aip)\cdot 4H_2O]_\infty$	0.2(1)	0.011(2)
$[Tb_2(aip)_3(H_2O)_{10}\cdot(aip)\cdot 4H_2O]_\infty$	32(3)	0.47(5)
$[Dy_2(aip)_3(H_2O)_{10}\cdot(aip)\cdot 4H_2O]_\infty$	0.6(1)	0.005(2)

RESULTS AND DISCUSSION

Crystal Structures Comparison. Both crystal structures are monodimensional and can be described as the juxtaposition of stair-like double molecular chains (See Figure 1).

In both crystal structures the double chain molecular motifs are strongly held together by a complex network of hydrogen bonds and π-stacking interactions to form stair-like molecular double-chains. These short intermolecular contacts are listed in Supporting Information Tables S3 and S4.

dx.doi.org/10.1021/ic402841d | Inorg. Chem. 2014, 53, 1217−1228

These double-chains are further interacting via hydrogen bonds and π-stacking interactions that involve the ligands which are located between the molecular double-chains (Figure 2).

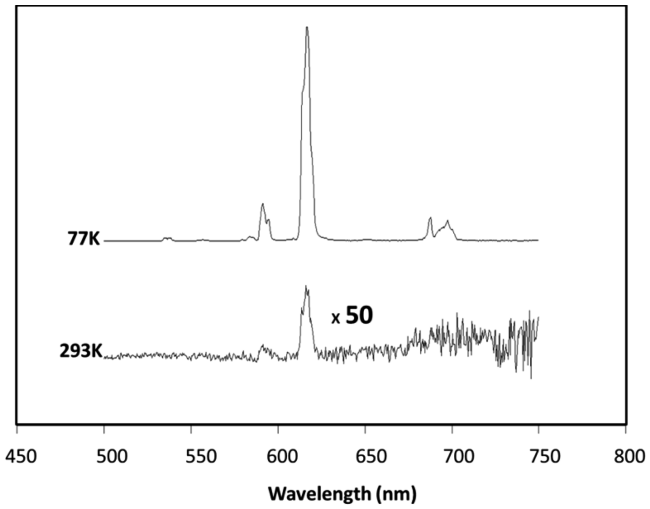

Figure 5. Emission spectra (λ_{exc} = 365 nm) for $[Eu_2(aip)_3(H_2O)_{10}\cdot(aip)\cdot 4H_2O]_\infty$ recorded at room temperature and at 77 K in similar experimental conditions. Spectrum recorded at room temperature is magnified (×50).

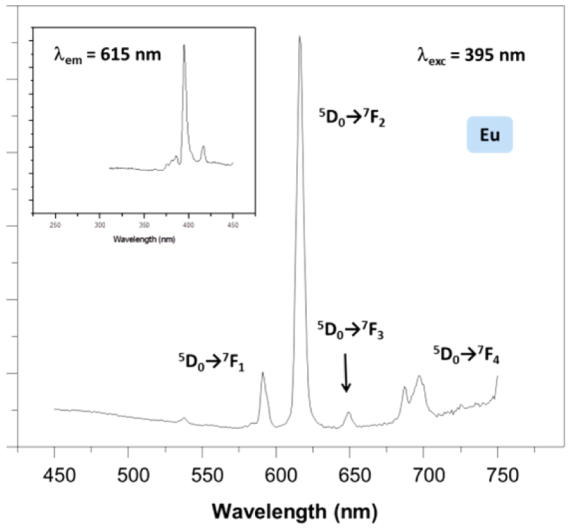

Figure 6. Excitation and emission spectra under direct excitation of the Eu^{3+} ion (λ_{exc} = 395 nm) of $[Eu_2(aip)_3(H_2O)_{10}\cdot(aip)\cdot 4H_2O]_\infty$.

These intermolecular contacts are listed in Supporting Information Tables S5 and S6.

The intermetallic distances between lanthanide ions that belong to the same double chain molecular motif are similar in both crystal structures (see Figures 3 and 4).

For both crystal structures, the distances between lanthanide ions that belong to different double-chain-like molecular motifs are quite long. The closest contacts are reported in Table 4.

This structural analysis confirms that the slight structural differences are not enough for explaining the observed differences between the luminescent properties.

Luminescent Properties of the Homonuclear Compounds $[Ln_2(ip)_3(H_2O)_9\cdot 6H_2O]_\infty$ with Ln = Sm−Dy. When exposed under UV radiation, some of these homonuclear compounds emit visible light (Supporting Information Figure S1). Excitation and emission spectra have been recorded for $[Ln_2(ip)_3(H_2O)_9\cdot 6H_2O]_\infty$ with Ln = Sm to Dy except Gd (Supporting Information Figure S12). All excitation spectra show broad bands from isophthalate ligand around 300 nm. This confirms the sensitization of the luminescence of the Ln^{3+} ions through the ligand. The emission spectrum of the Sm-containing compound exhibits typical $^4G_{5/2} \rightarrow {}^6H_J$ (J = 5/2−11/2) and is dominated by the $^4G_{5/2} \rightarrow {}^6H_{7/2}$ and $^4G_{5/2} \rightarrow {}^6H_{9/2}$ transitions at 598 and 641 nm, respectively. The emission spectrum of the Eu-containing compound displays typical Eu^{3+} transitions ($^5D_0 \rightarrow {}^7F_J$ J = 0−6) and is dominated by the $^5D_0 \rightarrow {}^7F_2$ transition centered at 615 nm. The spectrum of the Tb-based compound features the characteristic $Tb^{3+5}D_4 \rightarrow {}^7F_J$ (J = 6−0) transitions and is dominated by the $^5D_4 \rightarrow {}^7F_5$ transition at 545 nm. Finally, emission of the Dy-based compound arises from the $Dy^{3+4}F_{9/2} \rightarrow {}^6H_J$ (J = 15/2−9/2) and is dominated by the $^4F_{9/2} \rightarrow {}^6H_{13/2}$ transition at 572 nm. These results are in perfect agreement with those that have already been reported.[40]

Luminescent quantum yields and lifetimes of these four compounds are listed in Table 5. For all of them, the luminescent decay profiles are monoexponential. The weak luminescence of the Sm- and Dy-based compounds can be related to their small energy gaps.[47] In contrast, the Eu- and Tb-based coordination polymers present quite sizable quantum yields.

It is well-established that one of the most important processes that influences the luminescence properties of lanthanide ions in lanthanide-based coordination polymers is the intramolecular energy transfer that usually arises between the triplet state of the ligand and the lanthanide receiving levels.[48] The lowest excited singlet and triplet states have been estimated by referring to the wavelength of the UV−vis absorbance edge (320 nm ≈ 31250 cm^{-1}) and to the shortest wavelength of the phosphorescent band (425 nm ≈ 23 530 cm^{-1}) of the Gd-containing

Scheme 2. Suggested Luminescence Mechanisms for $[Eu_2(ip)_3(H_2O)_9\cdot 6H2O]_\infty$ (Left) and $[Eu_2(aip)_3(H_2O)_{10}\cdot(aip)\cdot 4H_2O]_\infty$ (Right)

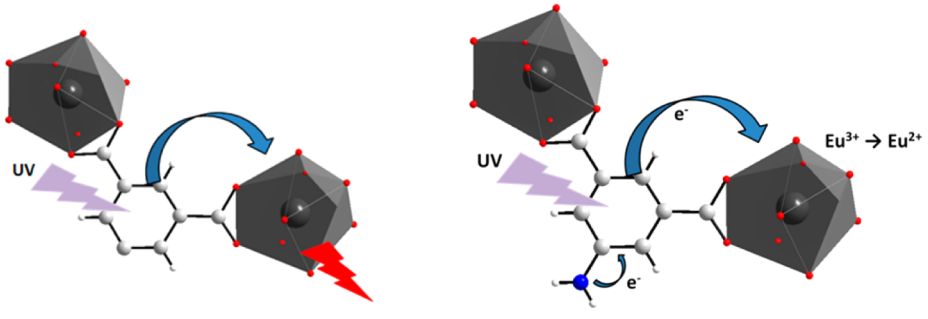

dx.doi.org/10.1021/ic402841d | Inorg. Chem. 2014, 53, 1217−1228

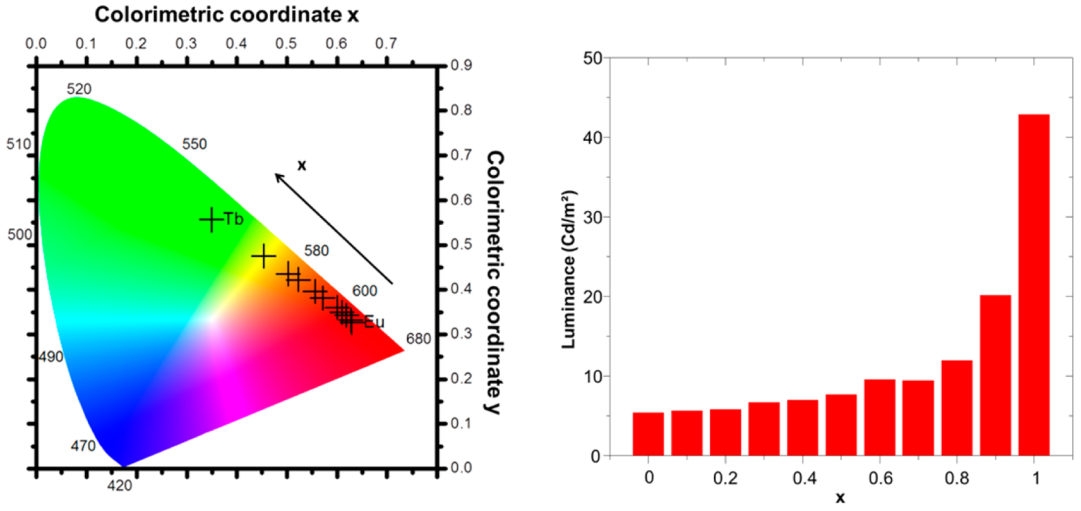

Figure 7. Colorimetric coordinates (left) and luminance (right) for some $[Eu_{2-2x}Tb_{2x}(ip)_3(H_2O)_9{\cdot}6H_2O]_\infty$ coordination polymers.

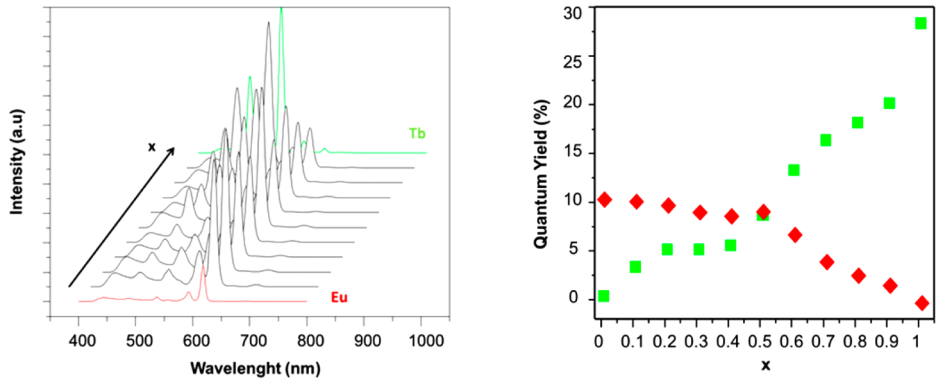

Figure 8. (Left) Luminescence spectra of some $[Eu_{2-2x}Tb_{2x}(ip)_3(H_2O)_9{\cdot}6H_2O]_\infty$ coordination polymers under UV irradiation (λ_{exc} = 312 nm) with $0 \le x \le 1$. (Right) Q_{Eu}^{ligand} (in red) and Q_{Tb}^{ligand} (in green) versus x for $[Eu_{2-2x}Tb_{2x}(ip)_3(H_2O)_9{\cdot}6H_2O]_\infty$ with $0 \le x \le 1$.

Table 8. Spectroscopic Data for $[Gd_1Tb_1(ip)_3(H_2O)_9{\cdot}6H_2O]_\infty$ and $[Eu_1Tb_1(ip)_3(H_2O)_9{\cdot}6H_2O]_\infty$

	Q_{Eu}^{ligand} (%)	τ_{obs} (ms)	Q_{Tb}^{ligand} (%)	τ_{obs} (ms)	τ_0 (ms)
$[Eu_1Tb_1(ip)_3(H_2O)_9{\cdot}6H_2O]_\infty$	8.3(8)	0.20(2)	11.1(10)	0.38(3)	
$[Gd_1Tb_1(ip)_3(H_2O)_9{\cdot}6H_2O]_\infty$			24.1(20)		0.65(6)

homologous compound (Supporting Information Figure S8).[49−51] According to Reinhoudt's empirical rules,[52] the intersystem crossing process is efficient when $\Delta E(^1\pi\pi^* - ^3\pi\pi^*)$ is greater than 5000 cm^{-1} which is the case here (ΔE = 7720 cm^{-1}). Moreover, according to Latva's rules,[53,54] the energy of the lowest excited triplet state of the ligand (23 530 cm^{-1}) is supposed to favor good ligand-to-metal energy transfer without significant back-transfer. This is in agreement with the quite sizable quantum yields that have been measured (Table 5). On the other hand, the luminance values of the Eu- and Tb-based compounds, 5(1) Cd m^{-2} and 43(1) Cd m^{-2}, respectively (see Supporting Information Table S1), are lower than those observed for other coordination polymers involving similar ligands.[26] This discrepancy between quantum yield and luminance can be related to the absorption ability of the ligand. Actually, the luminescence intensity depends on both the quantum yield and the molar absorption coefficient:

$$\Phi_{lum} \approx \varepsilon_\lambda \times Q_{ln}^{ligand} \quad (1)$$

Here, Φ_{lum} is the luminescence intensity, Q_{Ln}^{ligand} is the overall quantum yield, and ε_λ is the molar absorption coefficient at the excitation wavelength.[55]

Because of the insolubility in solvents of these coordination polymers, their molar absorption coefficients could not be measured which prevented us from estimating their luminescence intensity. Therefore, the molar absorption coefficient of the deprotonated ligand has been calculated from dilute aqueous solutions of its sodium salt: $\varepsilon_{\lambda max}$ = 670 L mol^{-1} cm^{-1} (see Supporting Information Figure S10). This quite low value[26] explains the moderate luminance of these compounds.

The efficiency of the overall ligand-to-metal energy transfer (η_{sens}) is also an important parameter. It is defined as the efficacy with which energy is transferred from the feeding levels of the ligand onto the lanthanide excited state:

$$Q_{ln}^{ligand} = \eta_{sens} \times Q_{ln}^{ln} = \eta_{sens} \times \frac{\tau_{obs}}{\tau_{rad}} \quad (2)$$

Here, Q_{Ln}^{ligand} is the overall quantum yield upon ligand excitation, Q_{Ln}^{Ln} the intrinsic quantum yield upon direct excitation of the

dx.doi.org/10.1021/ic402841d | Inorg. Chem. 2014, 53, 1217−1228

Scheme 3. Suggested Mechanism of Luminescence for $[Eu_1Tb_1(ip)_3(H_2O)_9{\cdot}6H_2O]_\infty$

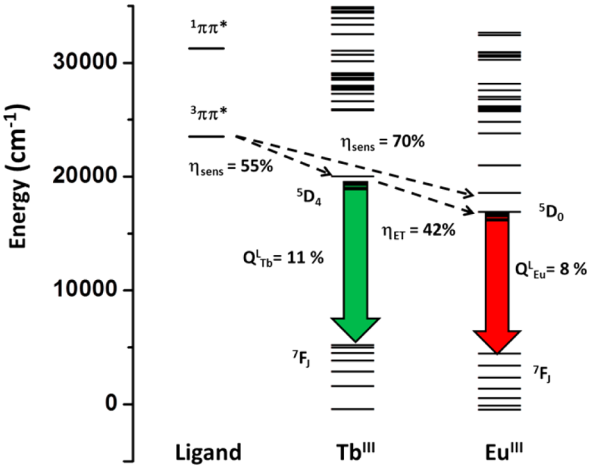

lanthanide ion, τ_{obs} the observed luminescent lifetime, and τ_{rad} the radiative luminescent lifetime.[56,57] The luminescence lifetimes and the intrinsic quantum yield have been measured for both the Tb- and the Eu-based coordination polymers (Table 6)[58] under excitation wavelengths that correspond to f−f transitions that do not overlap with the absorption band of the ligand: 395 nm ($^5D_3$ energy level for Eu^{3+}) and 380 nm ($^5D_3$ energy level for Tb^{3+}), respectively.[59,60]

In order to verify the reliability of these values we have used them for calculating the refractive index of the Eu-containing compound according to relation 4. The obtained value, n = 1.5(1), is in perfect agreement with what has already been measured for similar compounds.[25] These results indicate that isophthalate ligand is a good sensitizer for both Eu^{3+} and Tb^{3+} ions. On the other hand, Q_{Eu}^{Eu} is significantly lower than Q_{Tb}^{Tb}. This indicates that nonradiative deactivation of the Eu^{3+} is important. This can be related to the presence of 4.5 coordination water molecules per lanthanide ion. Indeed, it is known that the luminescence of Eu^{3+} ions is more sensitive to deactivation by O−H oscillators than that of Tb^{3+} ions.[56]

Luminescent Properties of the Homonuclear Compounds $[Ln_2(aip)_3(H_2O)_{10}{\cdot}(aip){\cdot}4H_2O]_\infty$ with Ln = Sm−Dy. When exposed under UV radiation, some of these homonuclear compounds emit visible light (see Supporting Information Figure S2). Excitation and emission spectra have been recorded for $[Ln_2(aip)_3(H_2O)_{10}{\cdot}(aip){\cdot}4H_2O]_\infty$ with Ln = Sm−Dy except Gd (Supporting Information Figure S13). All the excitation spectra but one for the Eu-based compound show broad bands from amino-isophthalate ligand around 365 nm. This confirms the sensitization of the luminescence of the Ln^{3+} ions through the ligand. The emission spectrum of the Sm-containing compound exhibits typical $^4G_{5/2} \rightarrow {}^6H_J$ (J = 5/2−9/2) and is dominated by the $^4G_{5/2} \rightarrow {}^6H_{7/2}$ and $^4G_{5/2} \rightarrow {}^6H_{9/2}$ transitions at 598 and 641 nm, respectively. The spectrum of the Tb-based compound features the characteristic $Tb^{3+5}D_4 \rightarrow {}^7F_J$ (J = 6−3) transitions and is dominated by the $^5D_4 \rightarrow {}^7F_5$ transition at 545 nm. Finally, emission of the Dy-based compound arises from the $Dy^{3+4}F_{9/2} \rightarrow {}^6H_J$ (J = 15/2−9/2) and is dominated by the $^4F_{9/2} \rightarrow {}^6H_{13/2}$ transition at 572 nm. These results are in perfect agreement with those that have already been reported.[41]

The luminescent quantum yields for $[Ln_2(aip)_3(H_2O)_{10}{\cdot}(aip){\cdot}4H_2O]_\infty$ with Ln = Sm, Tb, and Dy are listed in Table 7. The luminescent decay profiles are monoexponential.

The main difference between the luminescent properties of the two series of coordination polymers is the complete absence of luminescence for $[Eu_2(aip)_3(H_2O)_{10}{\cdot}(aip){\cdot}4H_2O]_\infty$ at room temperature.

On the basis of the absorption and phosphorescence spectra (see Supporting Information Figure S9) of the Gd-containing homologous coordination polymers, we have estimated the energy of the lowest singlet and triplet excited states of the amino-isophthalate ligand: $E(^1\pi\pi^*) \approx 375$ nm $\approx 26\,660$ cm^{-1} and $E(^3\pi\pi^*) \approx 505$ nm $\approx 19\,800$ cm^{-1}. Therefore, according to Reinhoudt's rule,[52] the intersystem crossing is supposed to be efficient ($\Delta E \approx 6860$ cm^{-1} > 5000 cm^{-1}). According to Latva's rules,[53] the energy of the lowest excited triplet state is also favorable to ligand-to-Tb energy transfer. The quantum yield (32%) and the luminance (47 Cd m^{-2}) of $[Tb_2(aip)_3(H_2O)_{10}{\cdot}(aip){\cdot}4H_2O]_\infty$ are close to that of $[Tb_2(ip)_3(H_2O)_9{\cdot}6H_2O]_\infty$ (28% and 43 Cd m^{-2}) although their respective molar absorption coefficients (670 L mol^{-1} cm^{-1} for $(ip)^{2-}$ and 2330 L mol^{-1} cm^{-1} for $(aip)^{2-}$ see Supporting Information Figure S11) are slightly different.

On the other hand, Latva's rules indicate that this lowest excited triplet state energy is also supposed to favor ligand-to-Eu energy transfer and therefore cannot explain the absence of luminescence.

Two well-known energy transfer mechanisms can explain this extinction of the Eu^{3+} luminescence: the back energy transfer Eu-to-ligand and the photoinduced electron transfer (PET). Both mechanisms are supposed to become less efficient when the temperature is lowered.[50] This is actually what we have observed (see Figure 5).

If back transfer was responsible of this phenomenon, it should arise even under direct excitation of the Eu^{3+}. Therefore, we have recorded the emission spectrum of $[Eu_2(aip)_3(H_2O)_{10}{\cdot}(aip){\cdot}4H_2O]_\infty$ with λ_{exc} = 395 nm which is the wavelength that corresponds to the excitation of the $^7F_0 \rightarrow {}^5D_3$ transition (Figure 6).

The measured overall quantum yield and luminescent lifetime are 8.8(8)% and 0.17(2) ms, respectively. They are in perfect agreement with what is observed for the homologous isophthalate-based compound (Q_{Ln}^{Ln} = 11(1)% and τ_{obs} = 0.12(2) ms). Therefore, it seems that back-transfer is not responsible of the absence of luminescence of $[Eu_2(aip)_3(H_2O)_{10}{\cdot}(aip){\cdot}4H_2O]_\infty$ under ligand excitation.

On the other hand, it is well-known that for easily reducible lanthanide ions a redox based mechanism can operate in which the first step is a photoinduced electron-transfer from the ligand to the lanthanide ion.[61,62] This mechanism is known for being efficient when $-NH_2$ electron donor groups are present in the vicinity of the lanthanide ion.[63] Therefore, PET mechanism is likely responsible of the absence of luminescence of $[Eu_2(aip)_3(H_2O)_{10}{\cdot}(aip){\cdot}4H_2O]_\infty$ under ligand excitation. Luminescence mechanisms suggested for the two Eu-containing coordination polymers described above are illustrated in Scheme 2.

In order to evaluate the influence of the PET mechanism on heteronuclear coordination polymers luminescence, we have undertaken the comparison of the luminescent properties exhibited by heterodinuclear coordination polymers that are isostructural to one or the other family.

Luminescent Properties of the Heteronuclear Coordination Polymers $[Eu_{2-2x}Tb_{2x}(ip)_3(H_2O)_9{\cdot}6H_2O]_\infty$ with $0 \le x \le 1$. Heteronuclear coordination polymers with general chemical formula $[Eu_{2-2x}Tb_{2x}(ip)_3(H_2O)_9{\cdot}6H_2O]_\infty$ with $0 \le x \le 1$ have been synthesized and characterized. Their colorimetric

dx.doi.org/10.1021/ic402841d | Inorg. Chem. 2014, 53, 1217−1228

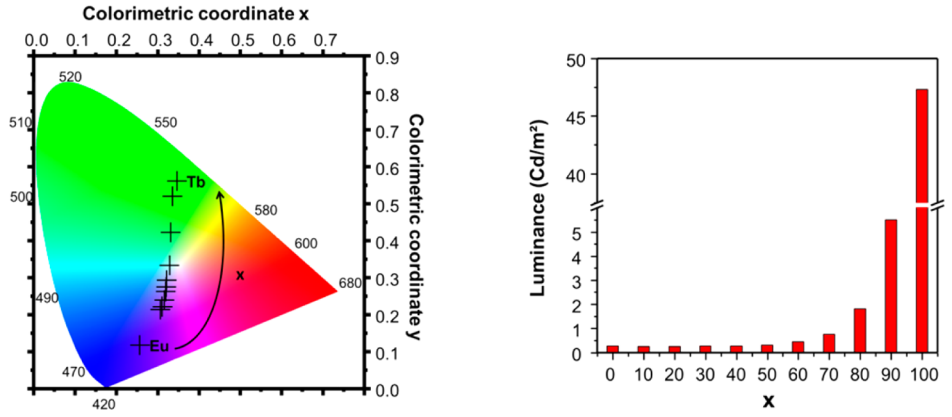

Figure 9. Colorimetric coordinates (left) and luminance (right) for some $[Eu_{2-2x}Tb_{2x}(aip)_3(H_2O)_{10}\cdot(aip)\cdot 4H_2O]_\infty$ compounds.

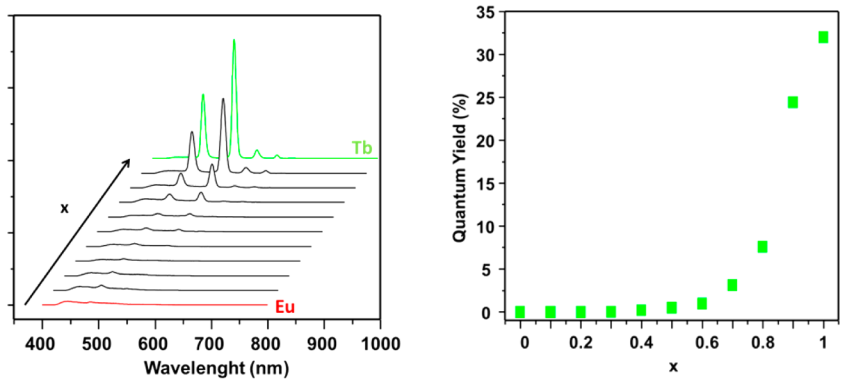

Figure 10. Luminescence spectra of some $[Eu_{2-2x}Tb_{2x}(aip)_3(H_2O)_{10}\cdot(aip)\cdot 4H_2O]_\infty$ compounds under UV irradiation of the ligand (λ_{exc} = 365 nm) with $0 \le x \le 1$. Q_{Tb}^{ligand} versus x with $0 \le x \le 1$ (right). These overall quantum yields have been estimated as described previously.

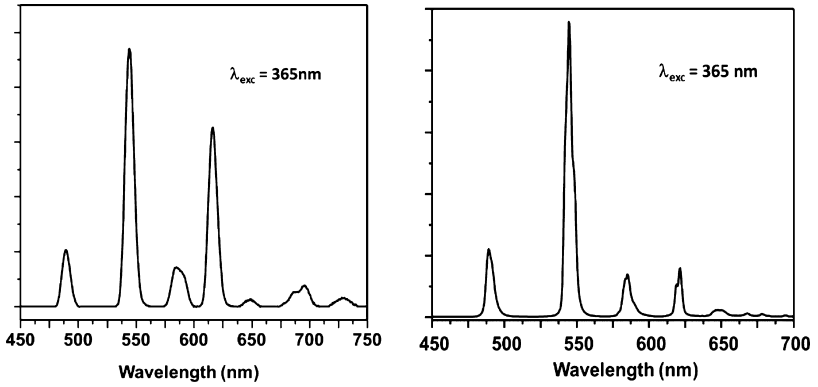

Figure 11. Emission spectra of $[Eu_1Tb_1(aip)_3(H_2O)_{10}\cdot(aip)\cdot 4H_2O]_\infty$ (left) and $[Gd_1Tb_1(aip)_3(H_2O)_{10}\cdot(aip)\cdot 4H_2O]_\infty$ (right). For both spectra λ_{exc} = 365 nm.

(Figure 7) and spectroscopic (Figure 8) properties have been measured. Numerical results are listed in Supporting Information Table S9.

This series of compounds presents a nonlinear evolution of the luminescent and colorimetric properties versus the Tb/Eu ratio. This is a classical behavior which has already been observed.[24−26]

The luminescent contributions to the total emission spectra of the Eu^{3+} and Tb^{3+} ions have been estimated on the basis of the $^5D_0 \rightarrow {}^7F_0$ and $^5D_4 \rightarrow {}^7F_5$ transitions, respectively, because they do not overlap with any other transition. Considering that all the compounds are isostructural and that the lanthanide ions are randomly distributed over the metallic sites of the crystal structure, it has been assumed that the relative intensities of all the peaks are similar to what was observed for the homonuclear compounds. With this assumption, Q_{Eu}^{ligand} and Q_{Tb}^{ligand} have been estimated (Figure 8). These calculations show that the Tb-to-Eu intermetallic energy transfer is efficient for $x < 0.9$, that is, as soon as statistically one Eu^{3+} ion is present in the neighborhood of a Tb^{3+} ion.[28] This intermetallic energy transfer (η_{ET}) can be quantified using the following relationship:

$$\eta_{ET} = 1 - \frac{\tau_{obs}}{\tau_0} \quad (3)$$

Here, τ_{obs} and τ_0 are, respectively, the lifetimes in the presence and in the absence of an acceptor.[47] As the Gd^{3+} ion presents its first excited states above the luminescent levels of the Tb^{3+} ion

dx.doi.org/10.1021/ic402841d | Inorg. Chem. 2014, 53, 1217−1228

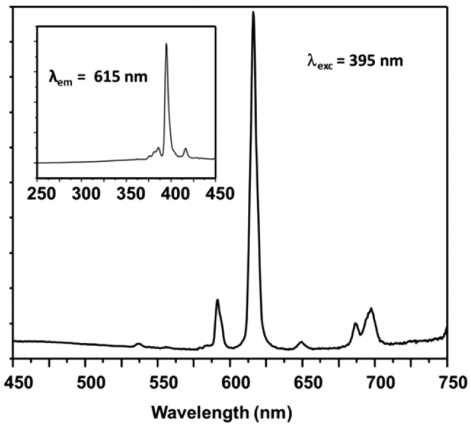

Figure 12. Emission spectrum of $[Eu_1Tb_1(aip)_3(H_2O)_{10}\cdot(aip)\cdot 4H_2O]_\infty$ under direct excitation of the Eu^{3+}. Excitation wavelength is 395 nm ($^5D_3$ energy level for Eu^{3+}). Inset shows the excitation spectrum.

and above the ligand triplet state, it cannot act as an acceptor. Therefore, we have synthesized $[Gd_1Tb_1(ip)_3(H_2O)_9\cdot 6H_2O]_\infty$ and $[Eu_1Tb_1(ip)_3(H_2O)_9\cdot 6H_2O]_\infty$ and studied their luminescent properties (Table 8). On the basis of these data, the intermetallic energy transfer can be estimated to 42(4)%. Luminescence spectra for both compounds are reported on Supporting Information Figures S14 and S15.

It can also be noticed in Table 8 that the overall quantum yield Q_{Tb}^{ligand} is 24(2)% for $[Gd_1Tb_1(ip)_3(H_2O)_9\cdot 6H_2O]_\infty$. This suggests that the Gd^{3+} acts as a spacer in this compound and reduces the Tb-to-Tb energy transfer by increasing the Tb−Tb mean distance.

In the frame of the assumption that the relative intensities of the different peaks of the emission spectra do not depend on the Eu/Tb ratio, neither does τ_{rad}. Indeed

$$\frac{1}{\tau_{rad}} = A_{MD} n^3 \frac{I_{tot}}{I_{MD}} \quad (4)$$

where A_{MD} is a constant equal to 14.65 s^{-1}, n is the refractive index, I_{tot} is the integrated emission of the $^5D_0 \rightarrow {}^7F_J$ ($J = 0-6$) transitions, and I_{MD} is the integrated emission of the $^5D_0 \rightarrow {}^7F_1$ transition.[64]

Therefore, in this assumption, the radiative lifetimes of the homonuclear compounds can be considered as a good approximation of the radiative lifetimes of all the isostructural Tb/Eu dinuclear derivatives. Thus, from eq 2, η_{sens} relative to Tb^{3+} and Eu^{3+} can be estimated to 55% and 70%, respectively, for $[Eu_1Tb_1(ip)_3(H_2O)_9\cdot 6H_2O]_\infty$. A schematic summary of the different energy transfers is suggested in Scheme 3.

These values are in perfect agreement with what has been recently observed on terephthalate-based heteronuclear coordination polymers.[26]

Luminescent Properties of the Heteronuclear Coordination Polymers $[Eu_{2-2x}Tb_{2x}(aip)_3(H_2O)_{10}\cdot(aip)\cdot 4H_2O]_\infty$ with $0 \le x \le 1$. Heteronuclear coordination polymers with general chemical formula $[Eu_{2-2x}Tb_{2x}(aip)_3(H_2O)_{10}\cdot(aip)\cdot 4H_2O]_\infty$ with $0 \le x \le 1$ have been synthesized and characterized. Their colorimetric (Figure 9) and spectroscopic (Figure 10) properties have been measured. Numerical results are listed in Supporting Information Table S10.

Obviously, this series of coordination polymers exhibits completely different luminescent properties than the previous series. Indeed, the luminance and the Tb^{3+} characteristic peak intensities decrease abruptly as soon as some Eu^{3+} ions are present. Moreover, no red component to the color emission arises even for high Eu^{3+}/Tb^{3+} ratios. This behavior supports the hypothesis of a strong intermetallic energy transfer between Tb^{3+} and Eu^{3+} followed by an efficient Eu^{3+} deactivation through a PET mechanism. Moreover, a broad band appears in the 400−500 nm range for Eu-containing coordination polymers (Figure 10). This band, that could be attributed to a ligand-to-metal charge transfer transition,[48] is responsible of the blue component of the color emission (Figure 9).

These spectra suggest that there is an efficient Tb-to-Eu intermetallic energy transfer (η_{ET}). Therefore, we have synthesized compounds $[Eu_1Tb_1(aip)_3(H_2O)_{10}\cdot(aip)\cdot 4H_2O]_\infty$ and $[Gd_1Tb_1(aip)_3(H_2O)_{10}\cdot(aip)\cdot 4H_2O]_\infty$. Their luminescent spectra were recorded and the luminescent lifetimes measured (Figure 11). It can be noticed that because of the low intensity of the spectra, it has not been possible to measure accurately the quantum yields. The observed luminescent lifetimes are, respectively, 0.061(6) and 0.435(40) ms. Then, with the same procedure as the one previously described, it has been estimated that η_{ET} = 86(8)%. This quite sizable value confirms our interpretation.

For $[Gd_1Tb_1(aip)_3(H_2O)_{10}\cdot(aip)\cdot 4H_2O]_\infty$, it has been possible to measure the overall quantum yield, $Q_{Tb}^{ligand} = 25(2)\%$. This value is quite high and confirms that Gd^{3+} ions can act as spacers that reduce the Tb-to-Tb energy transfer.

At last, we have recorded the emission spectra of $[Eu_1Tb_1(aip)_3(H_2O)_{10}\cdot(aip)\cdot 4H_2O]_\infty$ under direct excitation of the Eu^{3+} (Figure 12). The results support our hypothesis. Indeed, when the Eu^{3+} ion is excited directly, no PET occurs, and luminescence is observed.

CONCLUSIONS AND OUTLOOKS

Coordination polymer series that present isoreticular crystal structures are quite rare.[65] In this Article, the luminescence properties of two pseudoisoreticular coordination polymers series are compared, and an efficient PET process is evidenced for the aip^{2-}-based series. This mechanism is well-known and has already been employed for the design of pH sensors[66] or signaling systems for s-block metal ions.[67] This mechanism constitutes a drawback as far as the red luminescence of Eu^{3+} ion is targeted, but it can be an asset for accessing new emitted colors by heteronuclear coordination polymers. Moreover, luminescent lanthanide-based coordination polymers are also known for their use as tagger in fight against counterfeiting.[68] Obviously, playing with PET mechanism and intermetallic energy transfer could provide new systems with new optical properties usable in that field. Our group is currently working along this line.

ASSOCIATED CONTENT

Supporting Information

Projection view of an extended asymmetric unit of $[Gd_2(ip)_3(H_2O)_9\cdot 6H_2O]_\infty$. Colorimetric and luminance data upon UV irradiation (λ_{exc} = 312 nm) of $[Ln_2(ip)_3(H_2O)_9\cdot 6H_2O]_\infty$ with Ln = Sm, Eu, Gd, Tb, and Dy (Figure S1). Projection view of an extended asymmetric unit of $[Eu_2(aip)_2(H_2O)_{10}\cdot(aip)\cdot 4H_2O]_\infty$. Colorimetric and luminance data upon UV irradiation (λ_{exc} = 365 nm) of $[Ln_2(aip)_3(H_2O)_{10}\cdot(aip)\cdot 4H_2O]_\infty$ with Ln = Sm, Eu, Gd, Tb, and Dy (Figure S2). Colorimetric and luminance data for $[Ln_2(ip)_3(H_2O)_9\cdot 6H_2O]_\infty$ (Table S1) and $[Ln_2(aip)_3(H_2O)_{10}\cdot(aip)\cdot 4H_2O]_\infty$ (Table S2) with Ln = Sm, Eu, Gd, Tb, and Dy. Thermogravimetric analyses for $Na_2(ip)\cdot H_2O$ (Figure S3) and $Na_2(aip)\cdot H_2O$ (Figure S4). Experimental X-ray diffraction patterns for $[Ln_2(ip)_3(H_2O)_9\cdot 6H_2O]_\infty$ and $[Ln_2(aip)_3(H_2O)_{10}\cdot$

dx.doi.org/10.1021/ic402841d | Inorg. Chem. 2014, 53, 1217−1228

$(aip)\cdot 4H_2O]_\infty$ with Ln = Sm, Eu, Gd, Tb, and Dy (Figure S5). Powder X-ray diffraction patterns for some $[Eu_{2-2x}Tb_{2x}(ip)_3(H_2O)_9\cdot 6H_2O]_\infty$ and $[Eu_{2-2x}Tb_{2x}(aip)_2(H_2O)_{10}\cdot(aip)\cdot 4H_2O]_\infty$ compounds with $0.1 \leq x \leq 0.9$ (Figure S6). SEM pictures of $[Eu_{1.6}Tb_{0.4}(ip)_3(H_2O)_9\cdot 6H_2O]_\infty$ and $[Eu_{1.4}Tb_{0.6}(aip)_3(H_2O)_{10}\cdot(aip)\cdot 4H_2O]_\infty$ microcrystalline powders (Figure S7). Emission spectra of $[Gd_2(ip)_3(H_2O)_9\cdot 6H_2O]_\infty$ (Figure S8) and of $[Gd_2(aip)_3(H_2O)_{10}\cdot(aip)\cdot 4H_2O]_\infty$ (Figure S9) recorded at 77 K. Absorbance versus concentration of aqueous dilute solutions of the sodium salt of isophthalic acid (Figure S10) and of amino-isophthalic acid (Figure S11). Shortest interchain distances in a double chain molecular motif of $[Gd_2(ip)_3(H_2O)_9\cdot 6H_2O]_\infty$ (Table S3) and of $[Eu_2(aip)_2(H_2O)_{10}\cdot(aip)\cdot 4H_2O]_\infty$ (Table S4). Shortest interchain distances between double chain molecular motifs of $[Gd_2(ip)_3(H_2O)_9\cdot 6H_2O]_\infty$ (Table S5) and of $[Eu_2(aip)_2(H_2O)_{10}\cdot(aip)\cdot 4H_2O]_\infty$ (Table S6). Shortest intermetallic distances between lanthanide ions that belong to the same double chain molecular motif for $[Gd_2(ip)_3(H_2O)_9\cdot 6H_2O]_\infty$ (Table S7) and for $[Eu_2(aip)_2(H_2O)_{10}\cdot(aip)\cdot 4H_2O]_\infty$ (Table S8). Colorimetric and luminance data for $[Eu_{2-2x}Tb_{2x}(ip)_3(H_2O)_9\cdot 6H_2O]_\infty$ (Table S9) and for $[Eu_{2-2x}Tb_{2x}(aip)_2(H_2O)_{10}\cdot(aip)\cdot 4H_2O]_\infty$ (Table S10) with $0 \leq x \leq 1$. Excitation and emission spectra for $[Ln_2(ip)_3(H_2O)_9\cdot 6H_2O]_\infty$ with Ln = Sm, Eu, Tb, and Dy (Figure S12). Excitation and emission spectra for $[Ln_2(aip)_3(H_2O)_{10}\cdot(aip)\cdot 4H_2O]_\infty$ with Ln = Sm, Tb. and Dy (Figure S13). Luminescence spectrum for $[EuTb(ip)_3(H_2O)_9\cdot 6H_2O]_\infty$ (Figure S14) and for $[GdTb(ip)_3(H_2O)_9\cdot 6H_2O]_\infty$ (Figure S15). This material is available free of charge via the Internet at http://pubs.acs.org.

AUTHOR INFORMATION

Corresponding Author

*E-mail: Olivier.guillou@insa-rennes.fr. Phone: (+33) 2 23 23 84 38. Fax: (+33) 2 23 23 87 85.

Notes

The authors declare no competing financial interest.

ACKNOWLEDGMENTS

The China Scholarship Council Ph.D. Program and cooperation program with the French UT & INSA are acknowledged for financial support.

REFERENCES

(1) Czaja, A. U.; Trukhan, N.; Müller, U. *Chem. Soc. Rev.* **2009**, *38*, 1284−1293.
(2) Biradha, K.; Ramanan, A.; Vitall, J. J. *Cryst. Growth Des.* **2009**, *9*, 2969−2970.
(3) Eddaoudi, M.; Kim, J.; Rosi, N.; Vodak, D.; Wachter, J.; O'Keeffe, M.; Yaghi, O. M. *Science* **2002**, *295*, 469−472.
(4) Yaghi, O. M.; Li, G.; Li, H. *Nature* **1995**, *378*, 703−706.
(5) Yaghi, O. M.; Li, H. L. *J. Am. Chem. Soc.* **1995**, *117*, 10401−10402.
(6) Surblé, S.; Serre, C.; Millange, F.; Férey, G. *Solid State Sci.* **2006**, *8*, 413−417.
(7) Millange, F.; Serre, C.; Marrot, J.; Gardant, N.; Pelle, F.; Férey, G. *J. Mater. Chem.* **2004**, *14*, 642−645.
(8) Serre, C.; Millange, F.; Surblé, S.; Férey, G. *Angew. Chem., Int. Ed.* **2004**, *43*, 6286−6289.
(9) Kustaryono, D.; Kerbellec, N.; Calvez, G.; Daiguebonne, C.; Guillou, O. *Cryst. Growth Des.* **2010**, *10*, 775−781.
(10) Mu, B.; Li, F.; Huang, Y.; Walton, K. S. *J. Mater. Chem.* **2012**, *22*, 10172−10178.
(11) Kerbellec, N.; Daiguebonne, C.; Bernot, K.; Guillou, O.; Le Guillou, X. *J. Alloys Compd.* **2008**, *451*, 377−383.
(12) Lee, J.; Farha, O. K.; Roberts, J.; Scheidts, A.; Nguyen, S. T.; Hupp, J. T. *Chem. Soc. Rev.* **2009**, *38*, 1450−1459.
(13) Hamon, L.; Llewellyn, P. L.; Devic, T.; Ghoufi, A.; Clet, G.; Guillerm, V.; Pirngruber, G. D.; Maurin, G.; Serre, C.; Driver, G.; van Beek, W.; Jolimaitre, E.; Vimont, A.; Daturi, M.; Férey, G. *J. Am. Chem. Soc.* **2009**, *131*, 17490−17499.
(14) Bernot, K.; Luzon, J.; Caneschi, A.; Gatteschi, D.; Sessoli, R.; Bogani, L.; Vindigni, A.; Rettori, A.; Pini, M. G. *Phys. Rev. B* **2009**, *79*, 134419.
(15) Calvez, G.; Bernot, K.; Guillou, O.; Daiguebonne, C.; Caneschi, A.; Mahé, N. *Inorg. Chim. Acta* **2008**, *361*, 3997−4003.
(16) Jeon, J. R.; Clérac, R. *Dalton Trans.* **2012**, *41*, 9569−9586.
(17) Lan, A. J.; Li, K. H.; Wu, H. H.; Olson, D. H.; Emge, T. J.; Ki, W.; Hong, M. C.; Li, J. *Angew. Chem., Int. Ed.* **2009**, *48*, 2334−2338.
(18) Feng, J.; Zhang, H. J. *Chem. Soc. Rev.* **2013**, *42*, 387−410.
(19) Cui, Y.; Yue, Y.; Qian, G.; Chen, B. *Chem. Rev.* **2012**, 1126−1162.
(20) Cui, Y.; Xu, H.; Yue, Y.; Guo, Z.; Yu, J.; Chen, Z.; Gao, J.; Yang, Y.; Qian, G.; Chen, B. *J. Am. Chem. Soc.* **2012**, *134*, 3979−3982.
(21) Pellé, F.; Surblé, S.; Serre, C.; Millange, F.; Férey, G. *J. Lumin.* **2007**, *122*−*123*, 492−495.
(22) Serre, C.; Millange, F.; Thouvenot, C.; Gardant, N.; Pelle, F.; Ferey, G. *J. Mater. Chem.* **2004**, *14*, 1540−1543.
(23) Kerbellec, N.; Catala, L.; Daiguebonne, C.; Gloter, A.; Stephan, O.; Bünzli, J. C. G.; Guillou, O.; Mallah, T. *New J. Chem.* **2008**, *32*, 584−587.
(24) Kerbellec, N.; Kustaryono, D.; Haquin, V.; Etienne, M.; Daiguebonne, C.; Guillou, O. *Inorg. Chem.* **2009**, *48*, 2837−2843.
(25) Haquin, V.; Gumy, F.; Daiguebonne, C.; Bünzli, J. C. G.; Guillou, O. *Eur. J. Inorg. Chem.* **2009**, 491−497.
(26) Haquin, V.; Etienne, M.; Daiguebonne, C.; Freslon, S.; Calvez, G.; Bernot, K.; Le Polles, L.; Ashbrook, S. E.; Mitchell, M. R.; Bünzli, J. C. G.; Guillou, O. *Eur. J. Inorg. Chem.* **2013**, 3464−3476.
(27) Dang, S.; Zhang, J. H.; Sun, Z. M. *J. Mater. Chem.* **2012**, *22*, 8868−8873.
(28) Rodrigues, M. O.; Dutra, J. D. L.; Nunes, L. A. O.; de Sa, G. F.; de Azevedo, W. M.; Silva, P.; Paz, F. A. A.; Freire, R. O.; Junior, S. A. *J. Phys. Chem. C* **2012**, *116*, 19951−19957.
(29) Le Natur, F.; Calvez, G.; Daiguebonne, C.; Guillou, O.; Bernot, K.; Ledoux, J.; Le Polles, L.; Roiland, C. *Inorg. Chem.* **2013**, *52*, 6720−6730.
(30) White, K. A.; Chengelis, D. A.; Gogick, K. A.; Stehman, J.; Rosi, N. L.; Petoud, S. *J. Am. Chem. Soc.* **2009**, *131*, 18069−18071.
(31) De Lill, D. T.; De Bettancourt-Dias, A.; Cahill, C. L. *Inorg. Chem.* **2007**, *46*, 3960−3965.
(32) Luo, Y.; Zheng, Y.; Calvez, G.; Freslon, S.; Bernot, K.; Daiguebonne, C.; Roisnel, T.; Guillou, O. *Cryst. Eng. Commun.* **2013**, *15*, 706−720.
(33) Harbuzaru, B. V.; Corma, A.; Rey, F.; Atienzar, P.; Jorda, J. L.; Garcia, H.; Ananias, D.; Carlos, L. D.; Rocha, J. *Angew. Chem., Int. Ed.* **2008**, *47*, 1080−1083.
(34) Matthes, P. R.; Höller, C. J.; Mai, M.; Heck, J.; Sedlmaier, S. J.; Schmiechen, S.; Feldmann, C.; Schnick, W.; Müller-Buschbaum, K. *J. Mater. Chem.* **2012**, *22*, 10179−10187.
(35) Cadiau, A.; Brites, D. S. C.; Costa, P. M. F. J.; Ferreira, R. A. S.; Rocha, J.; Carlos, L. D. *ACS Nano* **2013**, *7*, 7213−7218.
(36) Wang, Z.; Yang, Y.; Cui, Y.; Wang, Z.; Qian, G. *J. Alloys Compd.* **2012**, *510*, L5−L8.
(37) Fomina, I. G.; Dobrokhotova, Z. V.; Aleksandrov, G. G.; Zhilov, V. I.; Malkerova, I. P.; Alikhanyan, A. S.; Zhigunov, D. M.; Bogomyakov, A. S.; Gerasimova, V. I.; Novotortsev, V. M.; Eremenko, I. L. *Polyhedron* **2013**, *50*, 297−305.
(38) Guillou, O.; Daiguebonne, C. In *Handbook on the Physics and Chemistry of Rare Eaths*; Gschneider, K. A., Bünzli, J. C. G., Pecharsky, V. K., Eds.; Elsevier: Amsterdam, 2005; Vol. *34*, pp 359−404.
(39) Qiu, Y.; Daiguebonne, C.; Liu, J.; Zeng, R.; Kerbellec, N.; Deng, H.; Guillou, O. *Inorg. Chim. Acta* **2007**, *360*, 3265−3271.
(40) Daiguebonne, C.; Kerbellec, N.; Gérault, Y.; Guillou, O. *J. Alloys Compd.* **2008**, *451*, 372−376.

(41) Luo, Y.; Calvez, G.; Freslon, S.; Bernot, K.; Daiguebonne, C.; Guillou, O. *Eur. J. Inorg. Chem.* **2011**, 3705−3716.
(42) Kraus, W.; Nolze, G. *J. Appl. Crystallogr.* **1996**, *29*, 301−303.
(43) Roisnel, T.; Rodriguez-Carjaval, J. *Mater. Sci. Forum* **2000**, 308−313.
(44) Roisnel, T.; Rodriguez-Carjaval, J. *Materials Science Forum, Proceedings of the Seventh European Powder Diffraction Conference (EPDIC 7)* **2001**, 118−123.
(45) Wyszecki, G. In *Handbook of Optics*; Driscoll, W. G., Vaughan, W., Eds.; McGraw-Hill Book Company: New York, 1978; pp 1−15.
(46) CIE. *International Commission on Illumination—Technical Report*; 1995.
(47) Eliseeva, S. V.; Bünzli, J. C. G. *Chem. Soc. Rev.* **2010**, *39*, 189−227.
(48) Bünzli, J. C. G.; Eliseeva, S. V. In *Lanthanide Luminescence*; Hänninen, P., Härmä, H., Eds.; Springer: Berlin, 2010; pp 1−45.
(49) Shi, M.; Li, F.; Yi, T.; Zhang, D.; Hu, H.; Huang, C.-H. *Inorg. Chem.* **2005**, *44*, 8929−8936.
(50) Prodi, L.; Maestri, M.; Ziessel, R.; Balzani, V. *Inorg. Chem.* **1991**, *30*, 3798−3802.
(51) Quici, S.; Cavazzini, M.; Marzanni, G.; Accors, i. G.; Armaroli, N.; Ventura, B.; Barigelletti, F. *Inorg. Chem.* **2005**, *44*, 529−537.
(52) Steemers, F. J.; Verboom, W.; Reinhoudt, D. N.; Van der Tol, E. B.; Verhoeven, J. W. *J. Am. Chem. Soc.* **1995**, *117*, 9408−9414.
(53) Latva, M.; Takalo, H.; Mukkala, V.-M.; Matachescu, C.; Rodriguez-Ubis, J. C.; Kankare, J. *J. Lumin.* **1997**, *75*, 149−169.
(54) D'Aléo, A.; Pointillart, F.; Ouahab, L.; Andraud, C.; Maury, O. *Coord. Chem. Rev.* **2012**, *256*, 1604−1620.
(55) Bünzli, J.-C. G.; Comby, S.; Chauvin, A.-S.; Vandevyver, C. D. B. *J. Rare Earths* **2007**, *25*, 257−274.
(56) Comby, S.; Bünzli, J. C. G.; Gschneider, K. A.; Pecharsky, V. K. In *Handbook on the Physics and Chemistry of Rare Earths*; Elsevier: Amsterdam, 2007; Vol. *37*, pp 1−353.
(57) Werts, M. H. V.; Jukes, R. T. F.; Verhoeven, J. W. *Phys. Chem. Chem. Phys.* **2002**, *4*, 1542−1548.
(58) Arakcheeva, A.; Logvinovich, D.; Chapuis, G.; Morozov, V.; Eliseeva, S. V.; Bünzli, J. C. G.; Pattison, P. *Chem. Sci.* **2012**, *3*, 384−390.
(59) Carnall, W. T.; Fields, P. R.; Rajnak, K. *J. Chem. Phys.* **1968**, *49*, 4450−4455.
(60) Carnall, W. T.; Fields, P. R.; Rajnak, K. *J. Chem. Phys.* **1968**, *49*, 4447−4450.
(61) Bünzli, J.-C. G. *Chem. Rev.* **2010**, *110*, 2729−2755.
(62) Ward, M. D. *Coord. Chem. Rev.* **2007**, *251*, 1663−1677.
(63) Galaup, C.; Couchet, J.-M.; Bedel, S.; Tisnès, P.; Picard, C. *J. Org. Chem.* **2005**, *70*, 2274−2284.
(64) Chauvin, A. S.; Gumy, F.; Imbert, D.; Bünzli, J. C. G. *Spectrosc. Lett.* **2004**, *37*, 512−537.
(65) Min, Z.; Singh-Wilmot, M. A.; Cahill, C. L.; Andrews, M.; Taylor, R. *Eur. J. Inorg. Chem.* **2012**, 4419−4426.
(66) de Silva, A. P.; Gunaratne, H. Q. N.; Rice, T. E. *Angew. Chem., Int. Ed.* **1996**, *35*, 2116−2118.
(67) De Silva, A. P.; Fox, D. B.; Huxley, A. J. M.; Moody, T. S. *Coord. Chem. Rev.* **2000**, *205*, 41−57.
(68) Daiguebonne, C.; Guillou, O.; Kerbellec, N. French Patent FR2906393, 2006.